https://doi.org/10.5194/egusphere-2025-221
Preprint. Discussion started: 3 February 2025

The importance of stratocumulus clouds for projected warming patterns and circulation changes

Philipp Breul[1], Paulo Ceppi[1], and Peer Nowack[2,3]

[1]Department of Physics, Imperial College London, London, United Kingdom
[2]Institute of Theoretical Informatics, Karlsruhe Institute of Technology, 76131 Karlsruhe, Germany
[3]Institute of Meteorology and Climate Research (IMK-ASF), Karlsruhe Institute of Technology, 76131 Karlsruhe, Germany

Correspondence: Philipp Breul (pyb18@ic.ac.uk)

Abstract. Stratocumulus clouds are thought to exert a strong positive radiative feedback on climate change, but recent analyses suggest this feedback is widely under-represented in global climate models. To assess the broader implications of this model error for the modeled climate change responses, we investigate the impact of Pacific stratocumulus cloud feedback on projected warming patterns, equilibrium climate sensitivity and the tropical atmospheric circulation under increased CO_2 concentrations. Using the Community Earth System Model with modifications to enhance low cloud cover sensitivity to sea surface temperature (SST) anomalies in Pacific stratocumulus regions, we find increased tropical SST variability and persistence, a higher equilibrium climate sensitivity, an enhanced east–west warming contrast across the tropical Pacific, and a stronger slow-down of the Walker circulation under $4\times CO_2$ conditions. Our findings are supported by inter-model relationships across CMIP6 $4\times CO_2$ simulations. These results underscore the importance of accurately representing cloud feedback in climate models to predict future climate change impacts not only globally, but also on a regional scale, such as warming patterns or circulation change.

1 Introduction

Clouds play a major role in shaping both our current climate as well as future climate change through their impact on incoming shortwave radiation as well as outgoing terrestrial longwave radiation. Any external forcing on the climate system can potentially change cloud properties, feeding back on climate change. So far, this cloud feedback has been primarily studied in terms of its implications for *global-mean* surface temperature change, particularly the equilibrium climate sensitivity (ECS) (e.g., Zelinka et al., 2020; Myers et al., 2021; Ceppi and Nowack, 2021).

However, cloud feedback is potentially also key for the *pattern* of surface warming, influencing the local radiation budget and atmospheric circulation (e.g., Voigt and Shaw, 2015; Ceppi and Hartmann, 2016). This is all the more important as general circulation models (GCMs) feature a wide spread of sensitivity of low clouds to sea surface temperatures (SSTs) in stratocumulus regions, with most GCMs underestimating this sensitivity relative to observations (Myers et al., 2021; Ceppi et al., 2024).

In this study, we test the climate impact of increasing stratocumulus cloud sensitivity to SST in a coupled climate model in the Northeast and Southeast Pacific subsidence regions. These are of special interest as they couple to major climate modes in the

https://doi.org/10.5194/egusphere-2025-221
Preprint. Discussion started: 3 February 2025

Pacific (Bellomo et al., 2014; Rädel et al., 2016; Yuan et al., 2018; Myers and Mechoso, 2020). Our focus is on understanding the impact of enhanced low-cloud sensitivity on projected warming patterns and resulting circulation change.

2 Data and Methods

2.1 Experimental Setup

We use the Community Earth System Model version 2.1.3 (CESM2.1.3), with the atmosphere model CAM4 (Neale et al., 2010) and the ocean model POP2 (Danabasoglu et al., 2012). We use a T31 (3.8°) horizontal grid with 26 vertical levels for CAM4 and a 3°horizontal grid with 60 depth levels for POP2. Our choice of an already widely used model configuration with a relatively coarse spatial grid is aimed at computational efficiency when testing the effects of large-scale changes in cloud sensitivities to SSTs. Our primary goal is to qualitatively assess the importance of the role of clouds on coupled climate change, rather than achieving exact alignment with observations through our modifications to cloud sensitivities (see below).

In this CESM configuration, relative to observations, the sensitivity of low cloud fraction (LCC, defined as clouds at or lower than 700 hPa) to SST anomalies in Pacific subsidence regions is too low (Fig. A1). In parts of the subsidence regions, sensitivities even have the opposite sign compared to observations, causing the regional average to be close to zero (Fig. A2a). We thus modify the low cloud cover sensitivity to local SST, by adding an LCC perturbation at every radiation time step, proportional to the instantaneous SST anomaly. Importantly, this instantaneous perturbation is only applied to the LCC "seen" by the radiative transfer code, ensuring that any direct effect is only on the *radiative* properties of the cloud, and the perturbation is not carried over to the next time step. Instantaneous SST anomalies are calculated relative to the 450-year monthly climatology of the control simulation with unperturbed clouds, termed $1\times_{\text{Orig}}$ (Table 1). This setup is loosely similar to that of (Erfani and Burls, 2019). Although the CESM is biased in terms of its sensitivities to factors other than SST, the feedback is dominated by the SST contribution so we target that.

The LCC perturbation magnitude is set to -3 percentage points of local LCC anomaly per degree of local SST anomaly. This choice brings the LCC sensitivity into closer alignment with observations, despite a slight overshoot (Fig. A2a). Cloud sensitivities are calculated following the cloud-controlling factor analysis framework of Ceppi and Nowack (2021) and Ceppi et al. (2024), and we direct the reader there for more detail. The modifications are restricted to the Pacific subsidence regions as calculated from the ECMWF Reanalysis version 5 (ERA5; Hersbach et al., 2020), following Scott et al. (2020). The resulting regions are shown in Fig. A2b.

We use four different experimental setups, which are combinations of modified or unmodified cloud sensitivity and control or quadrupled CO_2 concentrations (Table 1). Comparing $1\times_{\text{Orig}}$ and $1\times_{\text{Mod}}$ allows us to analyze changes to internal variability. Comparing the $4\times CO_2$ responses with unperturbed versus perturbed clouds enables us to estimate the impact of enhanced cloud sensitivities under greenhouse gas (GHG) forcings. We spun up the model for 1250 years to reach equilibrium, then branched off and spun up $1\times_{\text{Orig}}$ and $1\times_{\text{Mod}}$ for an additional 50 years. The $4\times$CO2 experiments ($4\times$ Orig and $4\times_{\text{Mod}}$) include three 150-year ensemble members, branched off from their respective $1\times CO_2$ simulations at 150-year intervals to ensure approximate independence.

https://doi.org/10.5194/egusphere-2025-221
Preprint. Discussion started: 3 February 2025

Name	Cloud Modifications	CO_2	Length (years)	Ensemble Members
$1\times_{Orig}$	No	$1\times CO_2$	450	1
$1\times_{Mod}$	Yes	$1\times CO_2$	450	1
$4\times_{Orig}$	No	$4\times CO_2$	150	3
$4\times_{Mod}$	Yes	$4\times CO_2$	150	3

Table 1. Summary of the climate model experiments conducted.

2.2 CMIP6 data

In addition to our CESM experiments, we analyze monthly-mean output from 22 models from the Coupled Model Intercomparison Project Phase 6 (CMIP6; Eyring et al., 2016), using the piControl and $4\times CO_2$ experiments. The models were selected based on availability of necessary data for calculating the cloud-radiative sensitivity to SST anomalies, following the cloud-controlling factor analysis method of Ceppi and Nowack (2021). The models used are ACCESS-CM2, ACCESS-ESM1-5, BCC-CSM2-MR, BCC-ESM1, CESM2, CNRM-CM6-1, CNRM-ESM2-1, EC-Earth3-Veg, FGOALS-f3-L, GFDL-CM4, GISS-E2-1-G, HadGEM3-GC31-LL, INM-CM4-8, INM-CM5-0, IPSL-CM6A-LR, MIROC6, MIROC-ES2L, MPI-ESM1-2-HR, MPI-ESM1-2-LR, MRI-ESM2-0, NESM3, UKESM1-0-LL.

2.3 Definitions of Indices and Warming Patterns

We calculate the commonly-used Niño3.4 index as a measure of El Niño–Southern Oscillation (ENSO) strength, defined as the deseasonalised SST anomaly box-averaged over (5°S, 5°N) latitude and (190°E, 240°E) longitude (e.g., Trenberth and Stepaniak, 2001). To assess the Walker circulation strength we follow Vecchi et al. (2006) calculating the difference in surface pressure between two boxes: (5°S, 5°N) and (200°E, 280°E) in the equatorial East Pacific, minus (5°S, 5°N) and (80°E, 160°E) over the Indo-Pacific warm pool. For the index in the $4\times CO_2$ experiments we use anomalies relative to the corresponding $1\times CO_2$ experiments (noting that $1\times_{Mod}$ and $1\times_{Orig}$ have near-identical climatologies), as this allows us to compare between experiments and evaluate the evolution in the $4\times CO_2$ experiments. Finally, we calculate an index of Pacific east–west warming contrast as the difference of the same two box averages that are used to calculate the Walker circulation strength, but for surface temperature.

We calculate warming maps from $4\times CO_2$ experiments by regressing local surface temperature onto global-mean temperature. We will distinguish between fast, slow and total responses, calculated over the years 1–20, 21–150 and 1–150 since CO_2 quadrupling (as in e.g., Andrews et al., 2015; Rugenstein et al., 2016; Lin et al., 2019), respectively.

https://doi.org/10.5194/egusphere-2025-221
Preprint. Discussion started: 3 February 2025

3 Results

We first discuss the results from the two $1\times CO_2$ experiments $1\times_{\text{Orig}}$ and $1\times_{\text{Mod}}$, which allow us to analyse changes in internal variability stemming from the cloud sensitivity modifications. We will then turn our attention to the $4\times CO_2$ experiments $4\times_{\text{Orig}}$ and $4\times_{\text{Mod}}$. Finally, we will analyse the extent to which the results from these experiments hold across CMIP6 models.

3.1 Mean State and Internal Variability

Although changes to the mean state and internal variability are not the primary focus of this paper, results from the $1\times CO_2$ experiments enable us to test whether the cloud modifications result in behaviour in line with our physical understanding.

The climatological SSTs are almost unaffected between the $1\times_{\text{Orig}}$ and $1\times_{\text{Mod}}$ experiments (Fig. A3). While a few regions do show differences in SST, the corresponding anomalies are very small (~ 0.1K) and are located neither in the subsidence regions nor in the tropical Pacific. Changes in climatology are therefore unlikely to have a significant impact on the observed changes in internal variability discussed below.

The cloud modifications cause enhanced SST variance in the tropical Pacific and subtropical East Pacific (Fig. 1a). This behaviour is in line with our physical understanding of positive feedback between LCC and SSTs, which previous work established is not confined to local SST changes (e.g., Bellomo et al., 2014; Erfani and Burls, 2019; Zhou et al., 2017). Here, enhanced positive feedback between SST anomalies and LCC (locally, higher SSTs lead to lower LCC, which increases the SSTs) leads to locally more variable SSTs. In the equatorial Pacific, this enhanced variability is advected westward by the trade winds along the cold tongue region.

Due to the enhanced LCC–SST feedback, we find a higher SST variability in the Niño3.4 region and also an increase in extreme ENSO events, which is reflected in heavier tails of the estimated probability density of the Niño3.4 index (Fig. 1b). Additionally, ENSO becomes more persistent and larger in amplitude, which is reflected in an amplitude increase and a shift to lower frequencies of the power spectrum (Fig. 1c). Increased power is also found at periods of around a decade, suggesting possible changes in the amplitude of decadal Pacific variability. The IPO power spectrum (not shown) on the other hand shows reduced amplitude in response to enhanced low-cloud feedback, which points to a more complicated interaction on long timescales. We therefore leave a detailed investigation of such changes for future work. Overall, however, the findings shown in Fig. 1 are in agreement with the physical understanding of the enhanced feedback mechanisms detailed above.

3.2 Response to $4\times CO_2$ Forcing

We now analyze the impact of increased cloud sensitivity on the coupled climate response to $4\times CO_2$ forcing. As a first step, we estimate the effective radiative forcing (ERF) and equilibrium climate sensitivity (ECS) in the two experiments $4\times_{\text{Orig}}$ and $4\times_{\text{Mod}}$, by extrapolating the relationship between global-mean radiative imbalance and global-mean surface air temperature during the fast and slow response in each experiment (Fig. 2a; Gregory et al., 2004). We find $\text{ERF}_{\text{Orig}} = 7.35\,\text{Wm}^{-2}$ and $\text{ERF}_{\text{Mod}} = 7.26\,\text{Wm}^{-2}$, $\text{ECS}_{\text{Orig}} = 6.25\,\text{K}$ and $\text{ECS}_{\text{Mod}} = 6.63\,\text{K}$. The low-cloud modification therefore leaves ERF essentially unchanged (as expected given that our modification should only affect the SST-mediated cloud response; the small decrease is

https://doi.org/10.5194/egusphere-2025-221
Preprint. Discussion started: 3 February 2025

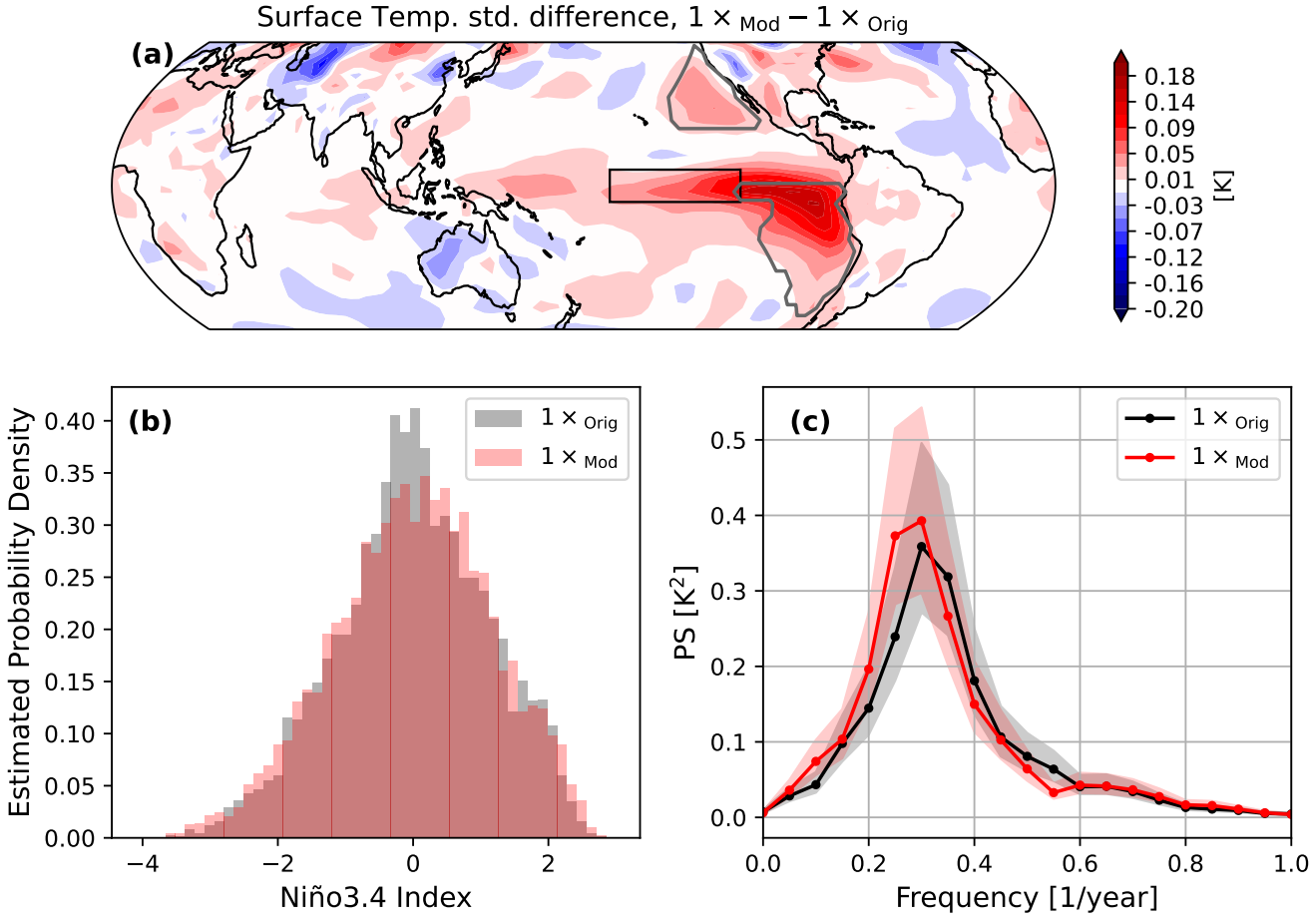

Figure 1. Changes to surface temperature variability between the $1\times_{\text{Mod}}$ and $1\times_{\text{Orig}}$ experiments. **(a)** Differences in surface temperature standard deviations. The grey contours denote the subsidence regions where the LCC sensitivity to SST anomalies was enhanced in the Mod experiments. The black box shows the Niño3.4 region. **(b)** Estimated probability densities of the Niño3.4 index. **(c)** Power spectrum of the Niño3.4 index, estimated using the Welch method (Welch, 1967) with 44 20-year long, half-overlapping windows. The shaded areas show 95% confidence intervals based on a χ^2-test.

https://doi.org/10.5194/egusphere-2025-221
Preprint. Discussion started: 3 February 2025

most likely sampling bias, as the ERF ranges between $4\times_{\text{Orig}}$ and $4\times_{\text{Mod}}$ completely overlap, Fig. 2a), while enhancing ECS by approximately 6.2%.

With the ERF unchanged, the change in ECS must come from climate feedback, which we calculate here as the slopes in Fig. 2a. Our expectation is for a more positive (or less negative) cloud feedback, and thus a less negative net feedback. We find a 7% decrease in net feedback magnitude in the fast $4\times CO_2$ response, in line with a higher ECS. The slow response only shows minimal change however, suggesting that the fast response is the main driver of global-mean warming differences. Considering clear-sky and cloud-radiative effect (CRE) feedbacks separately (Fig. A4a,b) reveals that the net feedback difference between $4\times_{\text{Orig}}$ and $4\times_{\text{Mod}}$ comes from the CRE component, which as expected is less negative in the fast response, while clear-sky feedback remains approximately unchanged. The CRE feedback is also more positive in $4\times_{\text{Mod}}$ in the slow response, although this is compensated by a similar and opposite change in clear-sky feedback. This difference in clear-sky feedback is due to different rates of sea ice loss and land albedo changes (not shown). It seems therefore likely that the compensation between cloud and non-cloud feedbacks is due to chance compensation of distinct processes, rather than reflecting a direct causal relationship between the two.

In our experiments with modified stratocumulus sensitivity to SST, the global climate feedbacks respond not only to the imposed change in low-cloud sensitivity, but also to any resulting changes in the SSTs themselves, both locally and potentially through a remote "pattern effect" (Andrews and Webb, 2018; Dong et al., 2019; Myers et al., 2023). To characterize the SST pattern response, we plot the east–west warming index (defined in Section 2.3), as a quantitative measure of the difference between East and West Pacific warming, against global-mean temperature in Fig. 2b. For both $4\times_{\text{Mod}}$ and $4\times_{\text{Orig}}$ experiments we observe a weakening of the east–west temperature difference, but this is stronger in the modified experiments (Fig. 2b).

Transitioning away from an index-based perspective, we show the warming pattern maps of $4\times_{\text{Orig}}$ for the fast, slow and total responses in Fig. 3a,b,c respectively. Our experiments show an enhanced East Pacific warming compared to other tropical regions, amplified Arctic warming in the fast response, and Antarctic amplification in the slow response. Similar fast and slow responses to CO_2 increase have been observed in previous studies (e.g., Andrews et al., 2015; Ceppi et al., 2018). Increasing the low-cloud sensitivities to SST results in a further enhancement of East Pacific warming, as shown by the fast, slow and total warming difference maps between $4\times_{\text{Mod}}$ and $4\times_{\text{Orig}}$ in Fig. 3d,e,f. This is in line with our physical expectation of an enhanced LCC–SST feedback, and consistent with our index-based warming contrast finding in Fig. 2b.

A weakening of the Walker circulation in response to CO_2 forcing has been documented in prior literature (Vecchi et al., 2006; He and Soden, 2015; Nowack et al., 2017; Malik et al., 2020; Heede et al., 2020). Enhanced East Pacific warming should weaken the circulation even further since the resulting impact on convection counteracts the Walker circulation (e.g. Tokinaga et al., 2012). This is indeed what we find in Fig. 2c: the Walker circulation weakens under CO_2 forcing (~ -20 Pa/K in the fast response and ~ -9 Pa/K in the slow response), but $4\times_{\text{Mod}}$ shows a greater weakening compared to $4\times_{\text{Orig}}$ (~ -34 Pa/K and ~ -14 Pa/K). This corresponds to $\sim 70\%$ additional reduction in the fast response and $\sim 49\%$ additional reduction in the slow response. We checked that differences in global mean lapse rate changes, which might cause Walker Circulation changes (Knutson and Manabe, 1995), are small (not shown) and are therefore unlikely to be the reason for the additional reduction.

https://doi.org/10.5194/egusphere-2025-221
Preprint. Discussion started: 3 February 2025

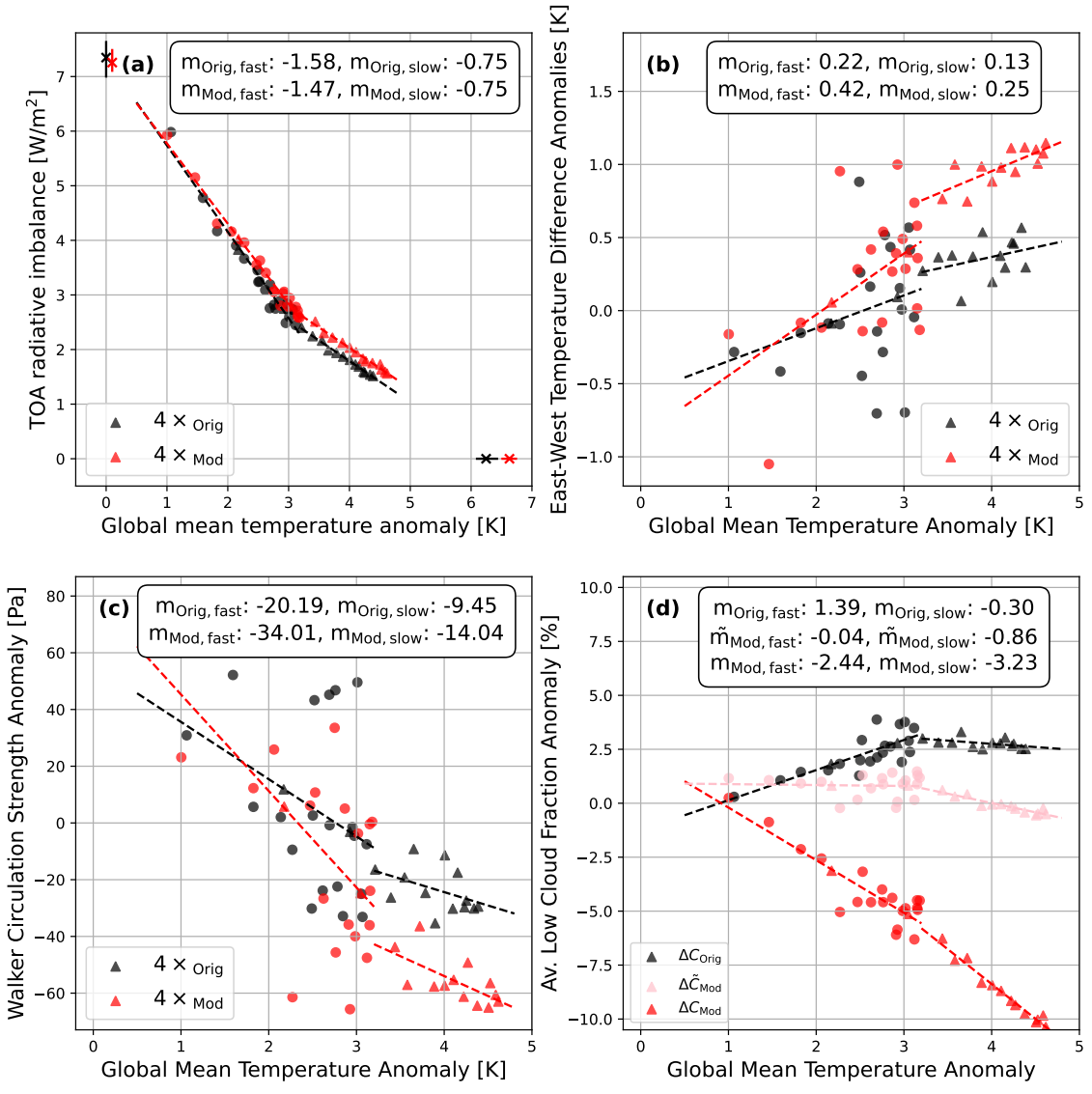

Figure 2. Ensemble-mean $4\times CO_2$ responses as a function of global-mean temperature anomaly. We show yearly averages for the first 20 years as dots and decadal averages as triangles over the complete 150 years, together with linear fits to both the fast and slow periods. We additionally plot the slope m for the fast and slow components. **(a)** Gregory plot of the top-of-the-atmosphere radiative imbalance plotted against global-mean temperature anomaly. The crosses show the mean projected equilibrium temperature on the x-axis and the approximated effective radiative forcing on the y-axis, with the vertical lines indicating ensemble spread. **(b)** East–west tropical Pacific warming contrast index plotted against global-mean temperature. **(c)** Same as (b) but for the Walker circulation strength index. **(d)** Anomalous low-cloud fraction averaged over the Pacific subsidence regions plotted against global mean temperature. Shown are the values of the $4\times_{\text{Orig}}$ experiments in black (C_{Orig}), the $4\times_{\text{Mod}}$ experiment in red (C_{Mod}) and the $4\times_{\text{Mod}}$ experiments without the extra SST sensitivity term in pink ($\tilde{C}_{\text{Mod}}$; see Section 3.3 and Eq. (6)).

https://doi.org/10.5194/egusphere-2025-221
Preprint. Discussion started: 3 February 2025

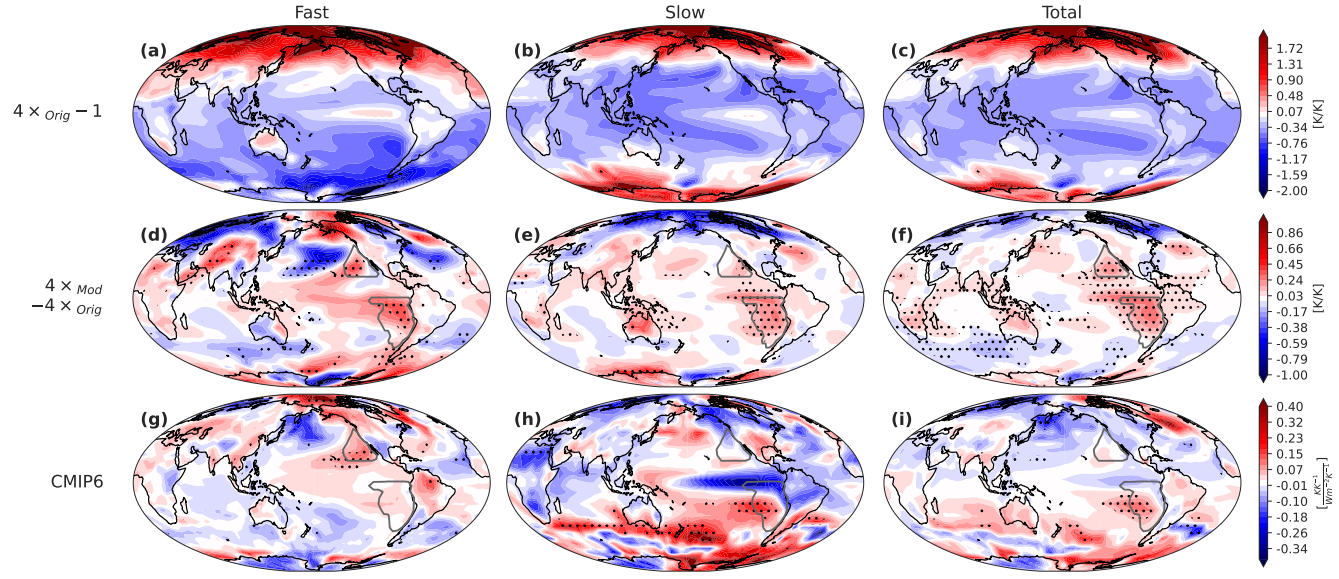

Figure 3. Warming patterns for **(a)** fast, **(b)** slow, and **(c)** total response of the $4\times_{\text{Orig}}$ experiments with 1 K/K (unit local per global surface warming) subtracted. **(d)-(f)** as (a)-(c) respectively but for the difference in warming pattern between $4\times_{\text{Mod}}$ and $4\times_{\text{Orig}}$. The stippling shows the regions where the signs of all nine possible differences between the two ensembles agree on the sign of change. **(g)** Fast, **(h)** slow, and **(i)** total CMIP6 across-model regression maps of warming patterns onto CRE–SST Pacific cloud sensitivity index. The stippling shows a statistical significance of $p < 0.05$, based on a Student t-test. Note that adjusting for multiple hypothesis testing following Wilks (2016) would remove any statistical significance.

3.3 Direct and pattern-mediated low-cloud responses

We now interpret the low-cloud feedback changes resulting from the LCC sensitivity perturbation. Because our GCM experiments are fully coupled, changes in cloud feedback between $4\times_{\text{Orig}}$ and $4\times_{\text{Mod}}$ result not only from the modified LCC sensitivities, but also from the coupled climate response to cloud feedback: modifying clouds changes the SST warming pattern, which in turn modifies the clouds further. Thus, our applied LCC sensitivity perturbation can affect low-cloud feedback in two ways:

- Through the imposed change in LCC sensitivity to SST; henceforth the "direct cloud response" to the LCC sensitivity perturbation;
- Through the change in SST warming pattern and its impact on cloud-controlling factors; henceforth the "pattern-mediated cloud response".

https://doi.org/10.5194/egusphere-2025-221
Preprint. Discussion started: 3 February 2025

To explain this further, we describe the total change in LCC as an expanded total derivative, following the cloud-controlling factor analysis framework (e.g., Stevens and Brenguier, 2009; Myers et al., 2021):

$$\frac{dC}{dT} = \frac{\partial C}{\partial S}\frac{dS}{dT} + \sum \frac{\partial C}{\partial Y_i}\frac{dY_i}{dT}, \tag{1}$$

with C the low-cloud cover in either of the $4\times CO_2$ experiments, T the corresponding global-mean surface temperature, S the SST, and Y_i any other relevant controlling factor; all variables are defined locally (except for T), but we drop the location index for conciseness. We also neglect $\frac{\partial C}{\partial T}$ as usual, since T is a global-mean quantity and therefore has no direct physical connection to local cloud cover.

We approximate the total derivatives in Eq. (1) by finite differences and get an approximate expression of LCC change,

$$\Delta C \approx \frac{\partial C}{\partial S}\Delta S + \sum \frac{\partial C}{\partial Y_i}\Delta Y_i. \tag{2}$$

We further assume that the cloud sensitivities (partial derivatives) are invariant in time and across experiments. The obvious exception is the sensitivity to SST, which we have modified between the Orig and Mod setup by adding a $\gamma = 3\%$ reduction in low cloud cover (in absolute percentage points) per unit SST increase. Using Eq. (2), we can therefore describe the changes in LCC in both $4\times_{\text{Orig}}$ and $4\times_{\text{Mod}}$ as

$$\Delta C_{\text{Orig}} \approx \frac{\partial C}{\partial S}\Delta S_{\text{Orig}} + \sum \frac{\partial C}{\partial Y_i}\Delta Y_{i,\text{Orig}}, \tag{3}$$

$$\Delta C_{\text{Mod}} \approx \left(\frac{\partial C}{\partial S} + \gamma\right)\Delta S_{\text{Mod}} + \sum \frac{\partial C}{\partial Y_i}\Delta Y_{i,\text{Mod}}. \tag{4}$$

Taking the difference of ΔC_{Mod} and ΔC_{Orig}, we obtain

$$\Delta C_{\text{Mod}} - \Delta C_{\text{Orig}} \approx \gamma\Delta S_{\text{Mod}} + \frac{\partial C}{\partial S}\left(\Delta S_{\text{Mod}} - \Delta S_{\text{Orig}}\right) + \sum \frac{\partial C}{\partial Y_i}\left(\Delta Y_{i,\text{Mod}} - \Delta Y_{i,\text{Orig}}\right). \tag{5}$$

We interpret the first term on the right-hand side of Eq. (5) as the direct cloud response; and the next two terms, involving changes to the cloud-controlling factors, as the pattern-mediated cloud response. To distinguish between the two, we introduce $\Delta\tilde{C}_{\text{Mod}}$, the interactive LCC calculated by the model in the $4\times_{\text{Mod}}$ experiments without the additional sensitivity to SST, such that $\Delta C_{\text{Mod}} = \Delta\tilde{C}_{\text{Mod}} + \gamma\Delta S_{\text{Mod}}$. This quantity is obtained as an extra output from our model runs. We can thus write:

$$\Delta\tilde{C}_{\text{Mod}} \approx \frac{\partial C}{\partial S}\Delta S_{\text{Mod}} + \sum \frac{\partial C}{\partial Y_i}\Delta Y_{i,\text{Mod}}. \tag{6}$$

The difference from ΔC_{Orig} therefore only contains the pattern-mediated response:

$$\Delta\tilde{C}_{\text{Mod}} - \Delta C_{\text{Orig}} \approx \frac{\partial C}{\partial S}\left(\Delta S_{\text{Mod}} - \Delta S_{\text{Orig}}\right) + \sum \frac{\partial C}{\partial Y_i}\left(\Delta Y_{i,\text{Mod}} - \Delta Y_{i,\text{Orig}}\right), \tag{7}$$

while the difference from ΔC_{Mod} only contains the direct response due to the SST sensitivity change:

$$\Delta C_{\text{Mod}} - \Delta\tilde{C}_{\text{Mod}} \approx \gamma\Delta S_{\text{Mod}}. \tag{8}$$

Comparing the changes in Eqs. (5), (7) and (8) therefore allows us to estimate the relative importance of direct and pattern-mediated responses on LCC.

https://doi.org/10.5194/egusphere-2025-221
Preprint. Discussion started: 3 February 2025

We plot ΔC_{Orig} (black), $\Delta \tilde{C}_{\text{Mod}}$ (pink) and ΔC_{Mod} (red) averaged over the Pacific subsidence region in Fig. 2d and estimate their change per unit global warming as the slopes for the fast and slow periods separately. While the LCC response evolves from moderately positive to weakly negative over the course of the $4\times_{\text{Orig}}$ experiment, in $4\times_{\text{Mod}}$ we instead observe a marked LCC decrease throughout. Comparing between ΔC_{Orig}, $\Delta \tilde{C}_{\text{Mod}}$ and ΔC_{Mod} additionally reveals that a substantial fraction of the change in LCC response is due to the SST pattern, and associated controlling factor responses. We quantify the importance of the pattern-mediated response (relative to the total LCC response to the SST sensitivity perturbation, $\Delta C_{\text{Mod}}/\Delta T$ minus $\Delta C_{\text{Orig}}/\Delta T$) as the change in Eq. (7) divided by that in Eq. (5), and normalized by global warming; this gives 0.37 for the fast response and 0.16 for the slow response.

By contrast, considering the near-global marine LCC response between 50°S and 50°N, we find near-identical $\Delta \tilde{C}_{\text{Mod}}$ and ΔC_{Orig} responses; the LCC change is almost entirely due to the direct response to the imposed SST sensitivity change (Fig. A4c). This suggests that pattern-mediated LCC decreases over the Pacific subsidence regions are compensated by non-local LCC *increases* in other regions. The lack of a global LCC response to the change in SST pattern suggests that this SST pattern change affects clouds primarily locally, rather than through changes in global lower-tropospheric stability mediated by remote SST changes in the warm pool. Consistent with this interpretation, the near-global EIS response over the ocean between 50°S and 50°N exhibits only modest changes between $4\times_{\text{Orig}}$ and $4\times_{\text{Mod}}$ (Fig. A4d).

In summary, our experiments show that, in CESM-CAM4, a higher and more realistic low-cloud sensitivity to SST leads to a greater decrease in low-cloud amount under abrupt $4\times CO_2$ increase. This occurs both directly, due to the increased low-cloud sensitivity to SST, and indirectly, through changes in the warming pattern and associated controlling factor changes. This SST pattern effect is important locally in the Pacific subsidence regions (enhancing the LCC reduction by a factor of about 1.5 in the fast response, and 1.2 in the slow response), but not globally, owing to the lack of a global change in lower-tropospheric stability.

3.4 CMIP6

We now analyse whether our experimental findings in the previous sections can also be traced in a CMIP6 model ensemble. As a first step we plot the ECS, derived from $4\times CO_2$ experiments, against the index of Pacific subsidence region cloud-radiative effect (CRE) SST sensitivity – where the SST sensitivity in each model is quantified through cloud-controlling factor analysis, as in Ceppi and Nowack (2021). We use CRE sensitivity in this section rather than LCC sensitivity owing to limited data availability of LCC output in CMIP6 models. In agreement with our findings in Fig. 2a, we find that a higher CRE sensitivity correlates with an increased ECS ($r = 0.67$), with an increase of $0.7\,\text{K}$ ($p = 0.001$) per unit CRE sensitivity increase (Fig. 4a). For comparison, we show the values calculated from the Orig and Mod experiments as black and red crosses, respectively. While the relationship between the CMIP models qualitatively fits our experiments, the former have a stronger dependency on the CRE sensitivity index. This is most likely due to CRE sensitivity in the Pacific subsidence regions correlating with CRE sensitivity in other regions in the CMIP6 models – whereas in our experiments the CRE sensitivity difference is restricted to the subsidence regions. As a side note, we find that our $4\times_{\text{Mod}}$ setup substantially overestimates CRE sensitivity to SST relative

https://doi.org/10.5194/egusphere-2025-221
Preprint. Discussion started: 3 February 2025

to observations (Fig. 4a), whereas this was only slightly the case for the LCC sensitivity (Fig. A2a). This difference may reflect a greater contribution of mid- and upper-level clouds on CRE in CESM-CAM4 compared to observations.

Next, we determine the impact of the CRE–SST sensitivity on the warming patterns across models. To this end, we regress the models' warming patterns against their CRE sensitivity averaged over the Pacific subsidence regions. Note that the maps in Fig. 3 have different units: for CMIP models (panels g–i) we regress onto a cloud-radiative sensitivity index in W m^{-2} K^{-1}, whereas for our model experiments (panels d–f) we are simply considering warming pattern differences. Nevertheless, the maps should be physically comparable, since in both cases we are considering the effect of an increase in cloud–SST sensitivity in the Pacific subsidence regions.

The fast response shows excellent agreement between our experiments (Fig. 3d) and the CMIP6 analysis (Fig. 3g), with similar patterns of enhanced warming in the East Pacific and reduced warming in the North and Southwest Pacific (though the latter feature is not as pronounced in our experiments). While the slow patterns (Fig. 3e,h) do not match as closely as the fast patterns, we still observe enhanced Southeast Pacific warming both in our experiments as well as in the CMIP6 analysis. The reduced warming along the cold-tongue region is in contrast to our experiments; however, this seems to be mostly driven by three outlier models (GISS-E2-1-G, MIROC6 and MIROC- ES2L) with exceptionally strong warming in this region. Excluding these three models reduces the effect significantly (Fig. A5). The total warming patterns (Fig. 3f,i) also show a qualitative agreement of enhanced East Pacific warming. In CMIP6, both the slow and total warming patterns include a hemispherically asymmetric component with enhanced warming in the Southern Hemisphere – likely related to changes in the Atlantic Meridional Overturning Circulation (Lin et al., 2019) – which is absent from our CESM simulations.

Given the increase in relative Southeast Pacific warming due to cloud feedback across CMIP6 models, we now turn to analyzing the relationship to Walker circulation change. Since a greater CRE–SST sensitivity is associated with an enhanced reduction in the east–west SST contrast across the tropical Pacific under CO_2 forcing (Fig. 3i), we expect an enhanced weakening of the Walker circulation. Figure 4b shows this is indeed the case, where we plot the slope of decadal averages of the Walker circulation anomaly per degree global-mean temperature change in the $4\times CO_2$ experiments against the Pacific subsidence region cloud sensitivity index. This gives a moderate Pearson correlation coefficient of $r = -0.48, p = 0.03$ and a decline of $-4.5\,\mathrm{Pa\ K^{-1}}$ per unit CRE sensitivity increase. We note however that two outlier models (namely MPI-ESM1-2-HR, MPI-ESM1-2-LR) were excluded from the analysis. The across-model relationship should therefore be considered with caution until the drivers of the large Walker circulation responses in the two MPI models are understood. Our experimental results (black and red crosses in Fig. 4b) agree with the CMIP6 inter-model regression, providing confidence that the relationship is causal. The higher CRE–SST sensitivity in observations compared to most models, therefore implies an enhanced weakening of the Walker Circulation in the future compared to model projections.

4 Conclusions

This study investigated the global climate impacts of increasing stratocumulus cloud sensitivity to sea surface temperature (SST) anomalies in the Pacific subsidence regions, targeting a common climate model bias (Myers et al., 2021; Ceppi et al.,

https://doi.org/10.5194/egusphere-2025-221
Preprint. Discussion started: 3 February 2025

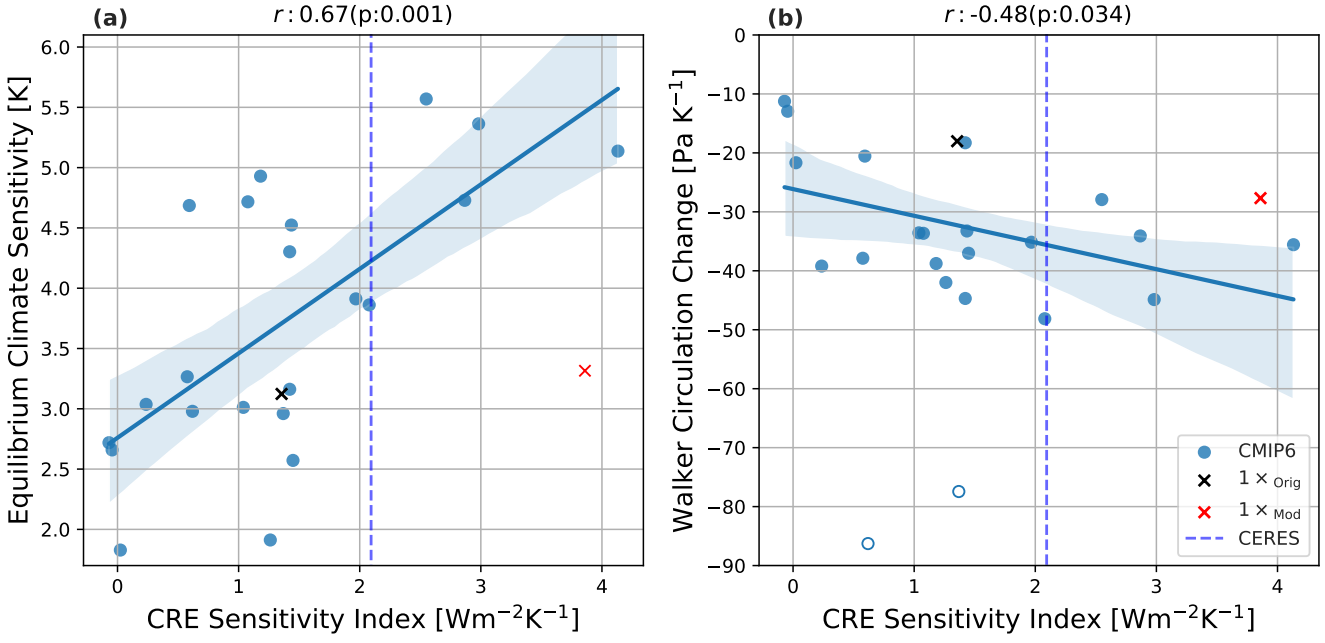

Figure 4. CMIP6 relationships between CRE–SST Pacific cloud sensitivity index and $4\times CO_2$ **(a)** Equilibrium Climate Sensitivity (ECS) and **(b)** Walker circulation change with global warming. The plot titles show the Pearson correlation coefficient r as well as its p-value, calculated using a Student t-test. The empty circles in (b) denote outliers that were excluded from the regression analysis. The dashed line shows the CRE sensitivity index calculated from CERES data. Black and red crosses show the values of the Orig and Mod experiments respectively.

2024). Our main focus was on warming patterns, the atmospheric circulation, and SST variability. We conducted simulations with modified low-cloud sensitivity under both $1\times CO_2$ and $4\times CO_2$ conditions, labelled as $1\times_{\text{Mod}}$ and $4\times_{\text{Mod}}$, and compared them to control simulations with default sensitivity, labelled $1\times_{\text{Orig}}$ and $4\times_{\text{Orig}}$.

The key impacts of stronger Pacific stratocumulus cloud feedback identified from our experiments are as follows:

- **Increased SST variability:** In the control climate, enhanced cloud sensitivity to SST leads to more variable, persistent, and extreme SSTs in the tropical and subtropical East Pacific, consistent with a positive feedback between low-cloud amount and SST.
- **Higher equilibrium climate sensitivity (ECS):** ECS increases by approximately 6% in $4\times_{\text{Mod}}$ compared to $4\times_{\text{Orig}}$, driven by a change in the climate feedback.
- **Change in SST warming pattern:** In addition to the ECS change, enhancing cloud sensitivity results in relatively higher warming in the East Pacific, and thus a reduced east–west contrast across the tropical Pacific under CO_2 forcing. This SST warming pattern acts to amplify the low-cloud reduction in the Pacific subsidence regions, by about 50% in the fast and 20% in the slow response.

https://doi.org/10.5194/egusphere-2025-221
Preprint. Discussion started: 3 February 2025

– **Walker circulation weakening:** Consistent with increased East Pacific warming, we observe an additional slowdown in Walker circulation.

To evaluate the broader implications of these findings, we compared our results with an across-model analysis of 22 CMIP6 models. We found a connection between ECS and Pacific subsidence cloud–SST sensitivity across models ($r = 0.67$, $p = 0.001$). Furthermore, through an inter-model regression analysis we found excellent alignment in terms of the fast warming pattern between our experiments and CMIP6 models. Agreement was more limited for the slow response, with discrepancies likely arising from model-dependent slower oceanic processes, such as changes in the Atlantic meridional overturning. This analysis indicates that our CESM findings have significant implications for climate projections, especially as models typically predict intensified warming in the East Pacific in the slow response to CO_2 forcing (Rugenstein et al., 2023), which may even further amplify the global impacts of stratocumulus feedback.

Additionally, we identified a potential across-model relationship in CMIP6 between cloud sensitivity and Walker circulation weakening ($r = -0.48$, $p = 0.03$, excluding two outlier models). This relationship agrees well with both our physical understanding and experimental results, suggesting that stratocumulus cloud sensitivity has substantial impacts on projected regional climate changes. This finding is especially important given that climate models still commonly exhibit biases in cloud feedback representation (Zelinka et al., 2022; Ceppi et al., 2024). Future work could address the importance of biases in other cloud types and their sensitivities to environmental factors, in particular high clouds and their effects on the atmospheric circulation (Wilson Kemsley et al., 2024).

Code and data availability. Data and Code will be made available at the end of the peer review process.

https://doi.org/10.5194/egusphere-2025-221
Preprint. Discussion started: 3 February 2025

Appendix A: Figures

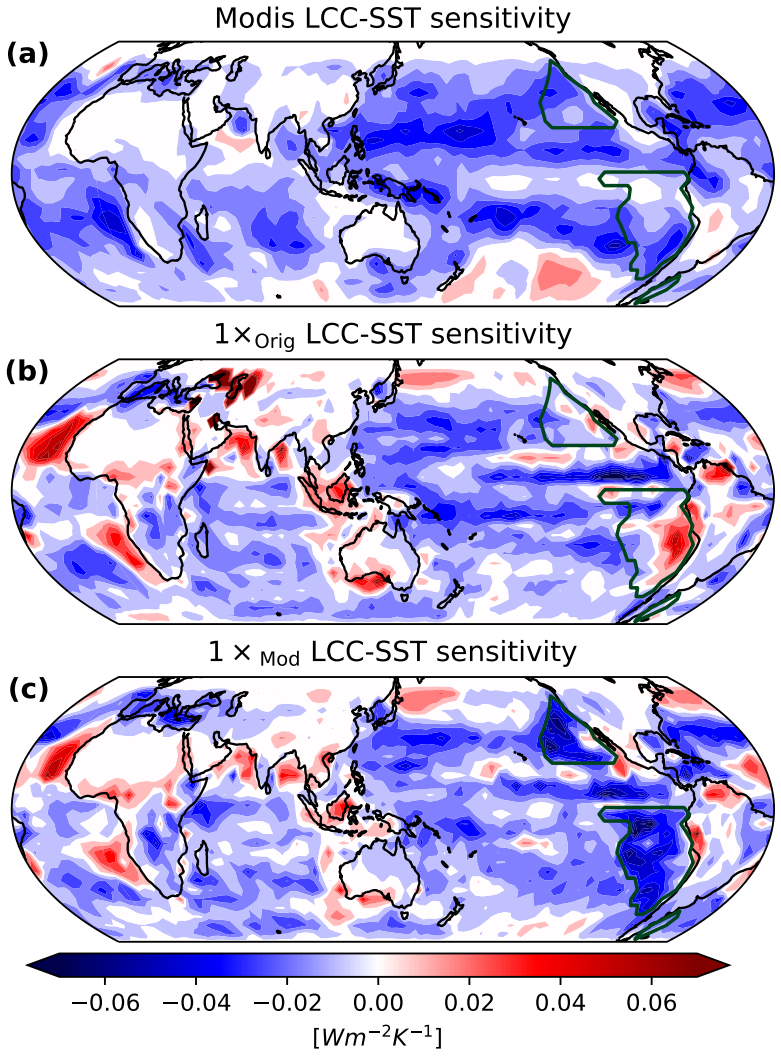

Figure A1. Sensitivities of low cloud cover (LCC) to surface temperature, for **(a)** MODIS observational data, **(b)** $1\times_{\text{Orig}}$ experiment and **(c)** $1\times_{\text{Mod}}$ experiment.

https://doi.org/10.5194/egusphere-2025-221
Preprint. Discussion started: 3 February 2025

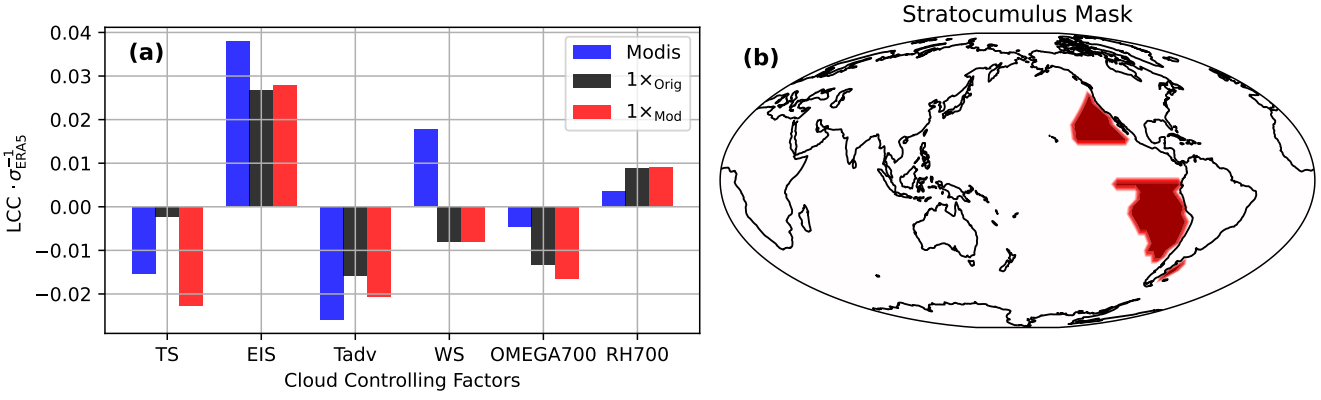

Figure A2. **(a)** Sensitivities of low cloud cover to controlling factors, expressed as percentage of low cloud cover per ERA5 standard deviation of each factor, averaged over Pacific subsidence regions. These sensitivities are presented for MODIS observations and for the $1\times_{\text{Orig}}$ and $1\times_{\text{Mod}}$ experiments. The controlling factors used are surface temperature (TS), estimated inversion strength (EIS), near-surface horizontal temperature advection (Tadv), near surface wind speed (WS), 700-hPa vertical velocity (OMEGA700) and 700-hPa relative humidity (RH700). **(b)** The Pacific subsidence regions, calculated from ERA5 following Scott et al. (2020).

https://doi.org/10.5194/egusphere-2025-221
Preprint. Discussion started: 3 February 2025

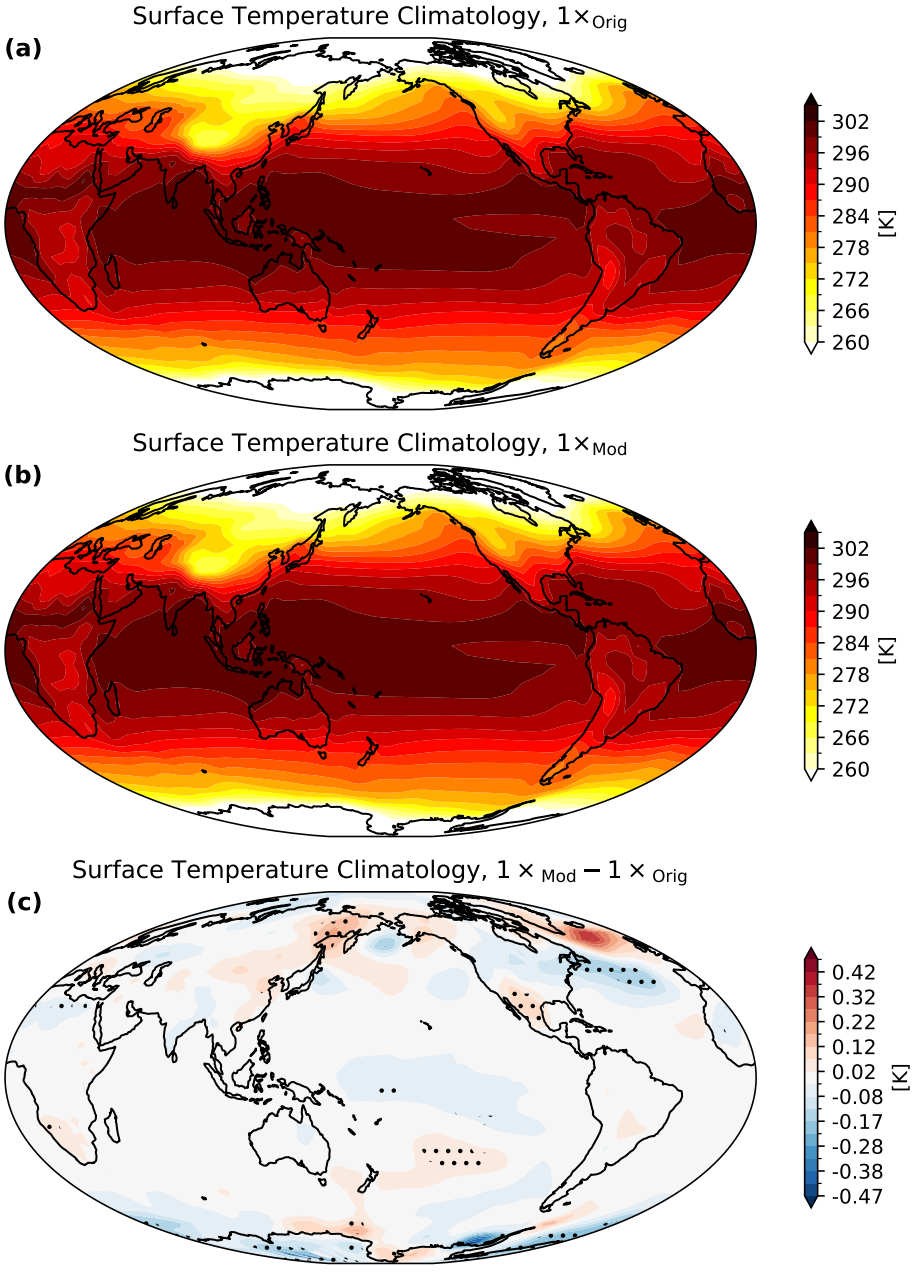

Figure A3. Climatological surface temperatures for **(a)** $1\times_{\text{Orig}}$, **(b)** $1\times_{\text{Mod}}$ and **(c)** their difference. The stippling in (c) marks significant differences at the $p < 0.05$ level using a two-sample t-test for autocorrelated data following Wilks (2019), on the annually averaged surface temperature.

https://doi.org/10.5194/egusphere-2025-221
Preprint. Discussion started: 3 February 2025

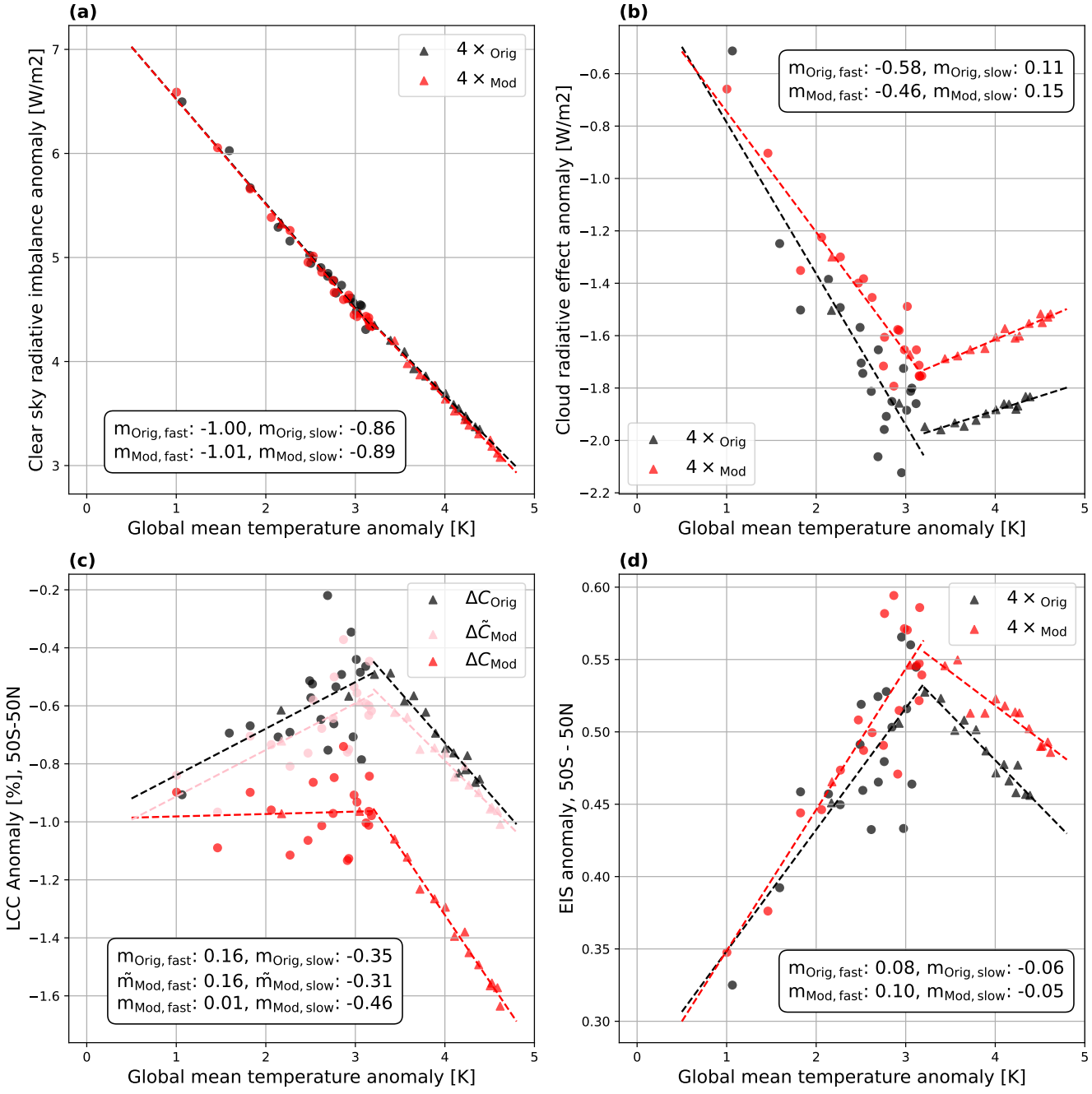

Figure A4. Same as Fig. 2, but for global-mean **(a)** clear-sky radiative fluxes and **(b)** cloud-radiative effect. **(c)** Low-cloud cover anomaly and **(d)** EIS anomaly, both averaged over the oceanic regions between 50°S to 50°N.

https://doi.org/10.5194/egusphere-2025-221
Preprint. Discussion started: 3 February 2025

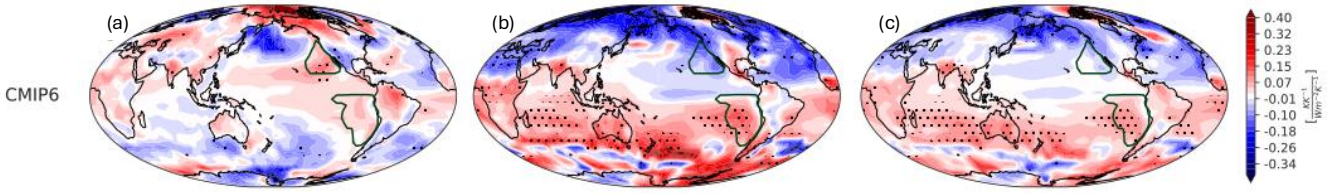

Figure A5. Same as Fig. A3 (g)(h)(i) but excluding GISS-E2-1-G, MIROC6 and MIROC-ES2L from the analysis.

https://doi.org/10.5194/egusphere-2025-221
Preprint. Discussion started: 3 February 2025

Author contributions. PB designed and performed the model experiments and analysis, and wrote the paper. PC contributed to the design of the experiments, interpretation of the results and the writing of the paper. PN contributed to the interpretation of the results and the writing of the paper.

Competing interests. At least one of the (co-)authors is a member of the editorial board of Atmospheric Chemistry and Physics.

Acknowledgements. We acknowledge support by UK Natural Environmental Research Council grants NE/V012045/1 (PC and PN), NE/T006250/1 (PC) and EP/Y036123/1 (PC). This work used JASMIN, the UK collaborative data analysis facility. This work used the ARCHER2 UK National Supercomputing Service (https://www.archer2.ac.uk). We acknowledge the World Climate Research Programme's Working Group on Coupled Modelling, which is responsible for CMIP, and we thank the climate modeling groups for producing and making available their model output. We also thank the Earth System Grid Federation (ESGF) for archiving the model output and providing access, and we thank the multiple funding agencies who support CMIP and ESGF.

https://doi.org/10.5194/egusphere-2025-221
Preprint. Discussion started: 3 February 2025

References

Andrews, T. and Webb, M. J.: The Dependence of Global Cloud and Lapse Rate Feedbacks on the Spatial Structure of Tropical Pacific Warming, Journal of Climate, 31, 641–654, https://doi.org/10.1175/JCLI-D-17-0087.1, publisher: American Meteorological Society Section: Journal of Climate, 2018.

Andrews, T., Gregory, J. M., and Webb, M. J.: The Dependence of Radiative Forcing and Feedback on Evolving Patterns of Surface Temperature Change in Climate Models, Journal of Climate, 28, 1630–1648, https://doi.org/10.1175/JCLI-D-14-00545.1, publisher: American Meteorological Society Section: Journal of Climate, 2015.

Bellomo, K., Clement, A., Mauritsen, T., Rädel, G., and Stevens, B.: Simulating the Role of Subtropical Stratocumulus Clouds in Driving Pacific Climate Variability, Journal of Climate, 27, 5119–5131, https://doi.org/10.1175/JCLI-D-13-00548.1, 2014.

Ceppi, P. and Hartmann, D. L.: Clouds and the Atmospheric Circulation Response to Warming, Journal of Climate, 29, 783–799, https://doi.org/10.1175/JCLI-D-15-0394.1, 2016.

Ceppi, P. and Nowack, P.: Observational evidence that cloud feedback amplifies global warming, Proceedings of the National Academy of Sciences, 118, e2026290 118, https://doi.org/10.1073/pnas.2026290118, 2021.

Ceppi, P., Zappa, G., Shepherd, T. G., and Gregory, J. M.: Fast and Slow Components of the Extratropical Atmospheric Circulation Response to CO_2 Forcing, Journal of Climate, 31, 1091–1105, https://doi.org/10.1175/JCLI-D-17-0323.1, 2018.

Ceppi, P., Myers, T. A., Nowack, P., Wall, C. J., and Zelinka, M. D.: Implications of a Pervasive Climate Model Bias for Low-Cloud Feedback, Geophysical Research Letters, 51, e2024GL110 525, https://doi.org/10.1029/2024GL110525, _eprint: https://onlinelibrary.wiley.com/doi/pdf/10.1029/2024GL110525, 2024.

Danabasoglu, G., Bates, S. C., Briegleb, B. P., Jayne, S. R., Jochum, M., Large, W. G., Peacock, S., and Yeager, S. G.: The CCSM4 Ocean Component, Journal of Climate, 25, 1361–1389, https://doi.org/10.1175/JCLI-D-11-00091.1, publisher: American Meteorological Society Section: Journal of Climate, 2012.

Dong, Y., Proistosescu, C., Armour, K. C., and Battisti, D. S.: Attributing Historical and Future Evolution of Radiative Feedbacks to Regional Warming Patterns using a Green's Function Approach: The Preeminence of the Western Pacific, Journal of Climate, 32, 5471–5491, https://doi.org/10.1175/JCLI-D-18-0843.1, publisher: American Meteorological Society Section: Journal of Climate, 2019.

Erfani, E. and Burls, N. J.: The Strength of Low-Cloud Feedbacks and Tropical Climate: A CESM Sensitivity Study, Journal of Climate, 32, 2497–2516, https://doi.org/10.1175/JCLI-D-18-0551.1, publisher: American Meteorological Society Section: Journal of Climate, 2019.

Eyring, V., Bony, S., Meehl, G. A., Senior, C. A., Stevens, B., Stouffer, R. J., and Taylor, K. E.: Overview of the Coupled Model Intercomparison Project Phase 6 (CMIP6) experimental design and organization, Geoscientific Model Development, 9, 1937–1958, https://doi.org/10.5194/gmd-9-1937-2016, 2016.

Gregory, J. M., Ingram, W. J., Palmer, M. A., Jones, G. S., Stott, P. A., Thorpe, R. B., Lowe, J. A., Johns, T. C., and Williams, K. D.: A new method for diagnosing radiative forcing and climate sensitivity, Geophysical Research Letters, 31, https://doi.org/10.1029/2003GL018747, _eprint: https://onlinelibrary.wiley.com/doi/pdf/10.1029/2003GL018747, 2004.

He, J. and Soden, B. J.: Anthropogenic Weakening of the Tropical Circulation: The Relative Roles of Direct CO2 Forcing and Sea Surface Temperature Change, Journal of Climate, 28, 8728–8742, https://doi.org/10.1175/JCLI-D-15-0205.1, publisher: American Meteorological Society Section: Journal of Climate, 2015.

https://doi.org/10.5194/egusphere-2025-221
Preprint. Discussion started: 3 February 2025

Heede, U. K., Fedorov, A. V., and Burls, N. J.: Time Scales and Mechanisms for the Tropical Pacific Response to Global Warming: A Tug of War between the Ocean Thermostat and Weaker Walker, Journal of Climate, 33, 6101–6118, https://doi.org/10.1175/JCLI-D-19-0690.1, publisher: American Meteorological Society Section: Journal of Climate, 2020.

Hersbach, H., Bell, B., Berrisford, P., Hirahara, S., Horányi, A., Muñoz-Sabater, J., Nicolas, J., Peubey, C., Radu, R., Schepers, D., Simmons, A., Soci, C., Abdalla, S., Abellan, X., Balsamo, G., Bechtold, P., Biavati, G., Bidlot, J., Bonavita, M., Chiara, G. D., Dahlgren, P., Dee, D., Diamantakis, M., Dragani, R., Flemming, J., Forbes, R., Fuentes, M., Geer, A., Haimberger, L., Healy, S., Hogan, R. J., Hólm, E., Janisková, M., Keeley, S., Laloyaux, P., Lopez, P., Lupu, C., Radnoti, G., Rosnay, P. d., Rozum, I., Vamborg, F., Villaume, S., and Thépaut, J.-N.: The ERA5 global reanalysis, Quarterly Journal of the Royal Meteorological Society, 146, 1999–2049, https://doi.org/https://doi.org/10.1002/qj.3803, 2020.

Knutson, T. R. and Manabe, S.: Time-Mean Response over the Tropical Pacific to Increased C02 in a Coupled Ocean-Atmosphere Model, Journal of Climate, 8, 2181–2199, https://doi.org/10.1175/1520-0442(1995)008<2181:TMROTT>2.0.CO;2, publisher: American Meteorological Society Section: Journal of Climate, 1995.

Lin, Y.-J., Hwang, Y.-T., Ceppi, P., and Gregory, J. M.: Uncertainty in the Evolution of Climate Feedback Traced to the Strength of the Atlantic Meridional Overturning Circulation, Geophysical Research Letters, 46, 12 331–12 339, https://doi.org/10.1029/2019GL083084, _eprint: https://onlinelibrary.wiley.com/doi/pdf/10.1029/2019GL083084, 2019.

Malik, A., Nowack, P. J., Haigh, J. D., Cao, L., Atique, L., and Plancherel, Y.: Tropical Pacific climate variability under solar geoengineering: impacts on ENSO extremes, Atmospheric Chemistry and Physics, 20, 15 461–15 485, https://doi.org/10.5194/acp-20-15461-2020, publisher: Copernicus GmbH, 2020.

Myers, T. A. and Mechoso, C. R.: Relative Contributions of Atmospheric, Oceanic, and Coupled Processes to North Pacific and North Atlantic Variability, Geophysical Research Letters, 47, e2019GL086 321, https://doi.org/10.1029/2019GL086321, _eprint: https://onlinelibrary.wiley.com/doi/pdf/10.1029/2019GL086321, 2020.

Myers, T. A., Scott, R. C., Zelinka, M. D., Klein, S. A., Norris, J. R., and Caldwell, P. M.: Observational constraints on low cloud feedback reduce uncertainty of climate sensitivity, Nature Climate Change, 11, 501–507, https://doi.org/10.1038/s41558-021-01039-0, 2021.

Myers, T. A., Zelinka, M. D., and Klein, S. A.: Observational Constraints on the Cloud Feedback Pattern Effect, Journal of Climate, 36, 6533–6545, https://doi.org/10.1175/JCLI-D-22-0862.1, publisher: American Meteorological Society Section: Journal of Climate, 2023.

Neale, R. B., Richter, J. H., Conley, A. J., Park, S., Lauritzen, P. H., Gettelman, A., Williamson, D. L., Rasch, P. J., Vavrus, S. J., Taylor, M. A., Collins, W. D., Zhang, M., and Lin, S.-J.: Description of the NCAR Community Atmosphere Model (CAM 4.0), 2010.

Nowack, P. J., Braesicke, P., Luke Abraham, N., and Pyle, J. A.: On the role of ozone feedback in the ENSO amplitude response under global warming, Geophysical Research Letters, 44, 3858–3866, https://doi.org/10.1002/2016GL072418, _eprint: https://onlinelibrary.wiley.com/doi/pdf/10.1002/2016GL072418, 2017.

Rugenstein, M., Zelinka, M., Karnauskas, K., Ceppi, P., and Andrews, T.: Patterns of Surface Warming Matter for Climate Sensitivity, Eos, 104, https://doi.org/10.1029/2023EO230411, 2023.

Rugenstein, M. A. A., Caldeira, K., and Knutti, R.: Dependence of global radiative feedbacks on evolving patterns of surface heat fluxes, Geophysical Research Letters, 43, 9877–9885, https://doi.org/10.1002/2016GL070907, _eprint: https://onlinelibrary.wiley.com/doi/pdf/10.1002/2016GL070907, 2016.

Rädel, G., Mauritsen, T., Stevens, B., Dommenget, D., Matei, D., Bellomo, K., and Clement, A.: Amplification of El Niño by cloud longwave coupling to atmospheric circulation, Nature Geoscience, 9, 106–110, https://doi.org/10.1038/ngeo2630, publisher: Nature Publishing Group, 2016.

https://doi.org/10.5194/egusphere-2025-221
Preprint. Discussion started: 3 February 2025

Scott, R. C., Myers, T. A., Norris, J. R., Zelinka, M. D., Klein, S. A., Sun, M., and Doelling, D. R.: Observed Sensitivity of Low-Cloud Radiative Effects to Meteorological Perturbations over the Global Oceans, Journal of Climate, 33, 7717–7734, https://doi.org/10.1175/JCLI-D-19-1028.1, publisher: American Meteorological Society Section: Journal of Climate, 2020.

Stevens, B. and Brenguier, J.-L.: Cloud-controlling Factors: Low Clouds, in: Clouds in the Perturbed Climate System, edited by Heintzenberg, J. and Charlson, R. J., pp. 173–196, The MIT Press, ISBN 978-0-262-25544-8, https://doi.org/10.7551/mitpress/8300.003.0010, 2009.

Tokinaga, H., Xie, S.-P., Deser, C., Kosaka, Y., and Okumura, Y. M.: Slowdown of the Walker circulation driven by tropical Indo-Pacific warming, Nature, 491, 439–443, https://doi.org/10.1038/nature11576, publisher: Nature Publishing Group, 2012.

Trenberth, K. E. and Stepaniak, D. P.: Indices of El Niño Evolution, Journal of Climate, 14, 1697–1701, https://doi.org/10.1175/1520-0442(2001)014<1697:LIOENO>2.0.CO;2, 2001.

Vecchi, G. A., Soden, B. J., Wittenberg, A. T., Held, I. M., Leetmaa, A., and Harrison, M. J.: Weakening of tropical Pacific atmospheric circulation due to anthropogenic forcing, Nature, 441, 73–76, https://doi.org/10.1038/nature04744, publisher: Nature Publishing Group, 2006.

Voigt, A. and Shaw, T. A.: Circulation response to warming shaped by radiative changes of clouds and water vapour, Nature Geoscience, 8, 102–106, https://doi.org/10.1038/ngeo2345, publisher: Nature Publishing Group, 2015.

Welch, P.: The use of fast Fourier transform for the estimation of power spectra: A method based on time averaging over short, modified periodograms, IEEE Transactions on Audio and Electroacoustics, 15, 70–73, https://doi.org/10.1109/TAU.1967.1161901, conference Name: IEEE Transactions on Audio and Electroacoustics, 1967.

Wilks, D.: Statistical methods in the atmospheric sciences, Elsevier Science, ISBN 978-0-12-816527-0, https://books.google.co.uk/books?id=VJqcDwAAQBAJ, 2019.

Wilks, D. S.: "The Stippling Shows Statistically Significant Grid Points": How Research Results are Routinely Overstated and Overinterpreted, and What to Do about It, Bulletin of the American Meteorological Society, 97, 2263–2273, https://doi.org/10.1175/BAMS-D-15-00267.1, 2016.

Wilson Kemsley, S., Ceppi, P., Andersen, H., Cermak, J., Stier, P., and Nowack, P.: A systematic evaluation of high-cloud controlling factors, Atmospheric Chemistry and Physics, 24, 8295–8316, https://doi.org/10.5194/acp-24-8295-2024, publisher: Copernicus GmbH, 2024.

Yuan, T., Oreopoulos, L., Platnick, S. E., and Meyer, K.: Observations of Local Positive Low Cloud Feedback Patterns and Their Role in Internal Variability and Climate Sensitivity, Geophysical Research Letters, 45, 4438–4445, https://doi.org/10.1029/2018GL077904, _eprint: https://onlinelibrary.wiley.com/doi/pdf/10.1029/2018GL077904, 2018.

Zelinka, M. D., Myers, T. A., McCoy, D. T., Po-Chedley, S., Caldwell, P. M., Ceppi, P., Klein, S. A., and Taylor, K. E.: Causes of Higher Climate Sensitivity in CMIP6 Models, Geophysical Research Letters, 47, e2019GL085 782, https://doi.org/10.1029/2019GL085782, _eprint: https://onlinelibrary.wiley.com/doi/pdf/10.1029/2019GL085782, 2020.

Zelinka, M. D., Klein, S. A., Qin, Y., and Myers, T. A.: Evaluating Climate Models' Cloud Feedbacks Against Expert Judgment, Journal of Geophysical Research: Atmospheres, 127, e2021JD035 198, https://doi.org/10.1029/2021JD035198, _eprint: https://onlinelibrary.wiley.com/doi/pdf/10.1029/2021JD035198, 2022.

Zhou, C., Zelinka, M. D., and Klein, S. A.: Analyzing the dependence of global cloud feedback on the spatial pattern of sea surface temperature change with a Green's function approach, Journal of Advances in Modeling Earth Systems, 9, 2174–2189, https://doi.org/10.1002/2017MS001096, _eprint: https://onlinelibrary.wiley.com/doi/pdf/10.1002/2017MS001096, 2017.